



Insights into Operational Stability and Processing of Halide Perovskite Active Layers

Journal:	<i>Energy & Environmental Science</i>
Manuscript ID	EE-ART-10-2018-003051.R2
Article Type:	Paper
Date Submitted by the Author:	18-Feb-2019
Complete List of Authors:	<p>Schelhas, Laura; Stanford Synchrotron Radiation Lightsource, Li, Zhen; National Renewable Energy Laboratory; Northwestern Polytechnical University, State Key Laboratory of Solidification Processing, Center for Nano Energy Materials, School of Materials Science and Engineering</p> <p>Christians, Jeffrey; National Renewable Energy Laboratory; Hope College</p> <p>Goyal, Anuj; Colorado School of Mines, Physics; National Renewable Energy Laboratory,</p> <p>Kairys, Paul; National Renewable Energy Laboratory</p> <p>Harvey, Steven; National Renewable Energy Laboratory</p> <p>Kim, DongHoe; National Renewable Energy Laboratory,</p> <p>Stone, Kevin; Stanford Synchrotron Radiation Laboratory,</p> <p>Luther, Joseph; National Renewable Energy Laboratory,</p> <p>Zhu, Kai; National Renewable Energy Laboratory, Chemical and Materials Science Center</p> <p>Stevanovic, Vladan; Colorado School of Mines, Physics</p> <p>Berry, Joseph; National Renewable Energy Laboratory (NREL), United States, National Center for Photovoltaics</p>

Insights into Operational Stability and Processing of Halide Perovskite Active Layers

Laura T. Schelhas¹, Zhen Li^{2,3}, Jeffrey A. Christians^{2,4}, Anuj Goyal⁵, Paul Kairys⁵, Steven Harvey², Dong Hoe Kim², Kevin H. Stone¹, Joseph M. Luther², Kai Zhu², Vladan Stevanovic⁵, Joseph J. Berry²

¹ SLAC National Accelerator Laboratory, Menlo Park, California 94025, United States.

² National Renewable Energy Laboratory, Golden, CO, 80401, United States.

³ State Key Laboratory of Solidification Processing, Center for Nano Energy Materials, School of Materials Science and Engineering, Northwestern Polytechnical University and Shaanxi Joint Laboratory of Graphene (NPU), Xi'an, 710072, P. R. China.

⁴ Hope College, Holland, MI 49423, United States.

⁵ Colorado School of Mines, Golden, CO, 80401, United States

Abstract (50-250 words):

Rapid improvement of the stability of metal halide perovskite materials is required to enable their adoption for energy production at Terawatt scale. To understand the role of the active layer stability in these devices we use *in-situ* x-ray diffraction to observe the evolution in structural stability across mixed A-site APbI₃ materials where the A-site, is a combination of formamidinium, Cs, and/or methylammonium. During device operation we observe spatial de-mixing and phase segregation into more pure constituent phases. Using complementary first-principles calculations of mixed A-site halide perovskites, a hypothesized framework explaining the experimentally observed mixing and de-mixing in these systems is presented and then validated using *in-situ* X-ray diffraction and spatially resolved time of flight secondary ion mass spectrometry. Taken together, these results indicate that stability is not only a function of device architecture or chemical formulation, but that the processing strategy is critically important in synthesizing the most energetically favorable state and therefore the most stable device systems. This study reconciles disparate reports within the literature and also highlights the limitations of shelf life studies to ascertain stability as well as the importance of testing devices under operational conditions.

Broader Context:

Perovskite solar cells appear poised on the brink of commercial success, yet there exist several potential roadblocks which could derail the prospects of this promising technology. At the forefront of these obstacles stands the strenuous stability demands for grid-scale photovoltaic applications. The perovskite, AMX₃, structure of halide perovskites has been shown previously to be amenable to extensive mixing at all three crystallographic sites. Particularly, mixed A-site compositions have been found to provide improved operational device stability relative to pure compositions; however, here we show, through a combination of experimental and theoretical results, that even these more stable mixed A-site perovskites can de-mix or phase segregate under stress into purer phase compositions, or constituent phases, which results in device degradation. Moreover, the developed theoretical framework indicates that processing strategy, as well as composition, will play a critical role in establishing homogeneity of the active layer materials during fabrication and

its subsequent maintenance during device operation to produce more stable halide perovskite devices.

Introduction:

In recent years, halide perovskite solar cells (PSC) have rapidly reached competitive power conversion efficiencies (PCEs) with certified values now in excess of 23% for single junction cells.^{1,2} The potential of PSCs to reach the terawatt level of renewable energy production is a result of their ability to be rapidly processed via solution or other scalable techniques³ as well as having highly tunable band gaps opening an avenue to high efficiencies at low cost.⁴ Although, halide perovskite semiconductors crystallize quite readily, the synthetic pathways taken during formation can greatly affect the resulting optoelectronic properties and ultimately the stability and performance of the devices. The synthetic complications can include but are not limited to precursor composition, ink concentrations and aging, heating profiles used during annealing, and the addition of additives to the precursor solutions. Optimizing these synthetic conditions is required to reproducibly generate high quality homogeneous films and has been the topic of many studies.^{5–12} Beyond the active layer, careful control over the different interfaces within the completed device is also very important. Ion mobility, resulting from the details of the active layer formation, and associated chemical incompatibilities with the contacting layers, makes the interfaces a region with high potential to initiate device failure.^{13,14} At the device level, stresses due to operation, such as varying temperature and electric fields can preferentially drive one or several degradation mechanisms simultaneously depending on the specific conditions.^{15–17} As the rapid increase in the power conversion efficiency of halide perovskite solar cells has begun to slow, a deeper mechanistic understanding of the PSC active layer formation and its integration into a high performance device stack is required. Additionally, understanding the materials subsequent behavior in operation has become integral in developing highly efficient, durable solar cells.¹⁸

PSCs crystallize in the perovskite, AMX_3 crystal structure where A is the monovalent cation (methylammonium, MA; formamidinium, FA; Rb, and/or Cs), M is the metal cation (Pb^{2+} and/or Sn^{2+}), and X is the halide anion (I^- , Cl^- , and/or Br^-). As the field has progressed, formulations of PSCs have evolved from the prototypical $MAPbI_3$ formulation to more complex mixed A-site and/or mixed halide compositions, (e.g. $Cs_xMA_yFA_{1-x-y}Pb(I_zBr_{1-z})_3$).^{19–23} With complex formulations, understanding the operation and stability of these materials becomes more challenging. For example, it is important to understand the geometric constraints of the lattice, commonly approximated by the Goldschmidt Tolerance Factor, when formulating new mixtures in order to target stable structures.^{19,24} Additionally, the composition and phase homogeneity within the film can also influence device performance.²⁵

PSCs of increasing complexity have been adopted for two main reasons. First, as previously noted, the band-gap is highly variable based on composition; therefore, these materials can be site-specifically tuned for use in tandem solar cell configurations.^{26–30} Second, despite the great initial PCE of PSCs, long term stability has been a challenge. MA has often been attributed as an unstable component of the prototypical $MAPbI_3$ formula, being relatively volatile and moisture

sensitive. Replacing MA with either FA or Cs alleviates the volatility issues, but at the expense of phase stability of the corner sharing octahedral perovskite phase. Pure FAPbI₃ tends to favor a hexagonal non-perovskite phase with edge sharing PbI₆⁴⁻ octahedra, whereas pure CsPbI₃ favors a non-perovskite orthorhombic phase with face sharing octahedra. Compositional mixing (e.g., mixing FA and Cs) to create ideal “average A-site radius values” that tune the tolerance factor has had success addressing these phase stability issues and in achieving shelf-stable compositions.¹⁹ Despite the success of the more complex mixtures, these materials can be susceptible to de-mixing and phase segregation into more pure compositions.

It is now well known that X-site substitutions of Br for I can both increase the bandgap but also result in photo-induced phase segregation, that while reversible is still problematic.^{31–34} However, it has been largely assumed that the success of the A-site mixing does not induce similar instabilities based on initial shelf-life studies.¹⁹ These systems also appear to have superior operational stability although the results are somewhat more mixed. Mixed cation devices have shown improved performance and stability^{21,35,36}; however, Domanski et al. have proposed that mobile cation vacancies can affect the long-term performance of PSCs.³⁷ Therefore, it is important to gain deeper understanding of the phase stability in mixed A-site PSCs and how the device performance and structure evolve over time under the stresses of operation. Here, utilizing a multi-modal approach, we simultaneously measure both the device output characteristics and structural properties to identify if and how phase segregation, or loss of crystallinity correlate with the device performance while in operation.

Using this multi-modal approach, we monitor the phase stability of mixed A-site, APbI₃ PSCs where A = FA, Cs, and/or MA in devices as they are subjected to constant illumination in humid conditions (~50% relative humidity), at room temperature for up to 15 hours. In the *in-situ* X-ray diffraction (XRD) measurements, taken while performing current/voltage (*I-V*) sweeps under illumination, we observe composition dependent degradation pathways which result in various degrees of phase segregated films depending on the PSC formulations. To identify the underlying energetic driver of this behavior, we calculated the Gibbs free energy of mixing in mixed A-site halide perovskites. We subsequently examine the implications of the developed theory-driven explanation to interpret other observations and elucidate the potential implications of the role of processing on enabling more structurally stable PSC materials and devices.

Results and Discussion:

The devices used for this study include a series of mixed A-site active layer compositions prepared using previously published methods.^{19,21} It should be noted that all perovskite materials discussed in this work contain only iodide at the X-site of the crystal structure to avoid complications arising from potential iodide/bromide phase segregation as discussed above. Details of the device preparations can be found in the SI. In summary, a compact TiO₂ layer of approximately 30 nm was deposited on patterned fluorine-doped tin oxide (FTO) coated glass substrates by spray pyrolysis at 450 °C. The perovskite active layer was deposited on the TiO₂ layer in a nitrogen flow box. Following annealing of the perovskite layer, a spiro-OMeTAD hole

transport layer was deposited by spin-coating. The films were then stored in dry air overnight and completed by deposition of an Au contact.

To understand the stability and degradation pathways of these devices we utilize *in-situ* X-ray diffraction (XRD) methods following previously published methods³⁸ and using the considerations outlined by Hoye and colleagues.³⁹ Within a custom built chamber (figure S1) at the Stanford Synchrotron Radiation Lightsource (SSRL), IV/XRD measurements are collected in a climate controlled chamber with relative humidity of ~50% (detailed experimental setup information can be found in the SI). The samples are illuminated using approximately 1-sun intensity from an Asahi Spectra Hal-320 Solar Simulator and *I-V* curves (forward and reverse) are collected, followed by a XRD scan. X-ray exposure is limited to 30 seconds per scan to limit beam induced degradation. The X-ray spot is positioned to collect data through the operating contact and this cycle is repeated every 15 minutes. To confirm the reproducibility of the synchrotron results, devices prepared under the same conditions were subjected to *ex situ* degradation, meaning there was no synchrotron X-ray exposure, at NREL under 1 sun illumination and similar environmental conditions using standard methods (ISOS-L1 conditions).⁴⁰ Non-synchrotron based XRD was taken before and after aging (figure S5) to verify that the results presented herein were not induced by the high intensity synchrotron radiation.

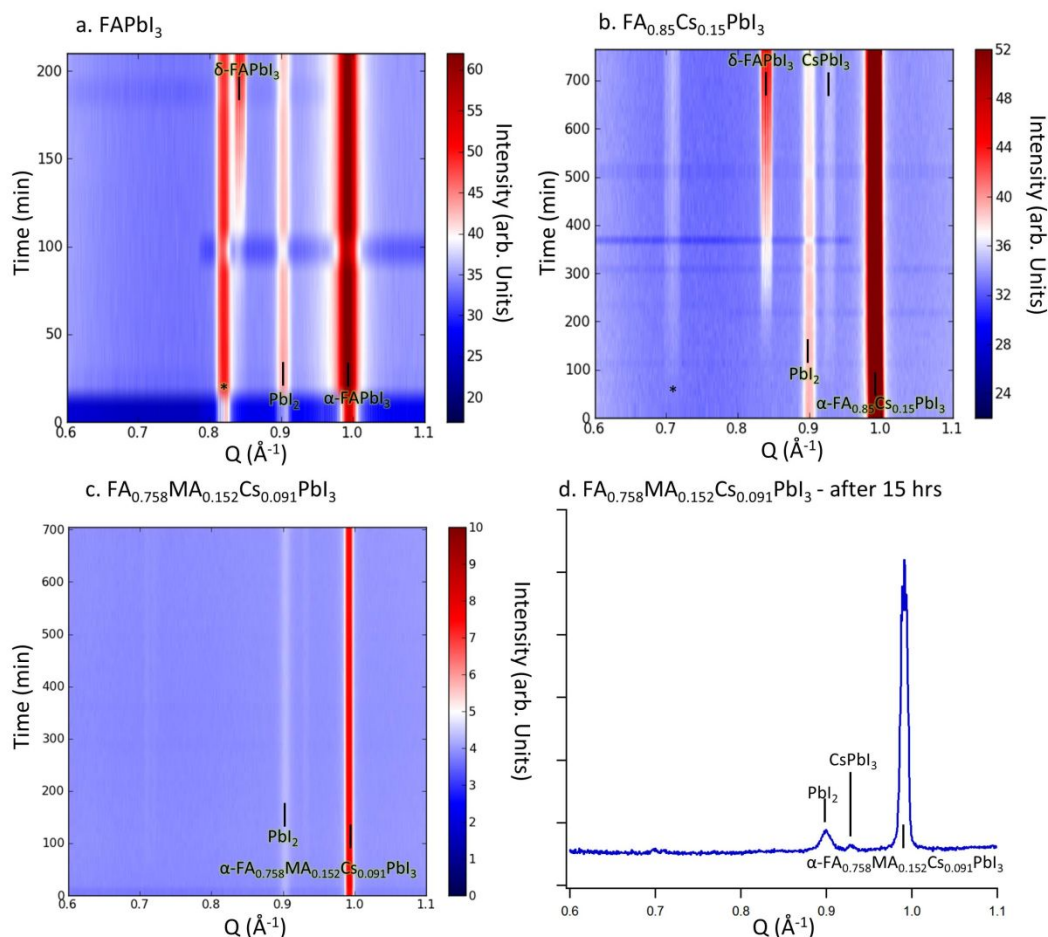


Figure 1. In-situ X-ray Diffraction of mixed A-site PSCs. X-ray diffraction profiles versus time of (a) FAPbI_3 , (b) $\text{FA}_{0.85}\text{Cs}_{0.15}\text{PbI}_3$, and (c) $\text{FA}_{0.758}\text{MA}_{0.152}\text{Cs}_{0.091}\text{PbI}_3$. The peak at $\sim 0.8 \text{ \AA}^{-1}$ (a) and 0.7 \AA^{-1} (b) is associated with a hydrate phase (marked by *). (d) XRD profile of $\text{FA}_{0.758}\text{MA}_{0.152}\text{Cs}_{0.091}\text{PbI}_3$ device after 15 hours of operation. Q is related to the diffraction angle (θ) and incident wavelength (λ) by $Q = (4\pi/\lambda) \sin\theta$. The X-ray wavelength used here was $\lambda = 0.9919 \text{ \AA}$.

The *in-situ* XRD results are summarized by contour plots in figure 1, and corresponding 2D scattering patterns of the initial and final scans are shown in figure S4. The scattering vector, Q , is plotted versus time to illustrate the evolution of crystalline phases in the active layers as a function of time. All samples show the presence of PbI_2 within the active layer. This excess PbI_2 has been observed previously and at low amounts does not significantly impact device PCE.¹⁹ The corresponding *in-situ* I - V curves for the devices in the reverse direction are shown in figure 2a-b, and figure S6 and the forward direction data are shown in figure S7, while complete device characteristics under AM1.5G irradiation can be found in Table S1. Corresponding I - V curves for the data presented in Table S1 can be found in figure S3. PV performance metrics (PCE, FF, V_{oc} , and I_{sc}) versus time are reported in figure S8 for the devices measured *in-situ*. These device data show consistent degradation trends to those seen using the *in-situ* system, validating this

unconventional method for device measurement and provides confirmation of the reproducibility of the results. The FAPbI_3 device (figure 1a and figure S6) initially shows the presence of the photoactive, corner-sharing “black” cubic, $\alpha\text{-FAPbI}_3$ phase, and also a hydrate phase, consistent with previous results.¹⁹ During operation the film begins to convert to the non-perovskite, edge-sharing “yellow”, hexagonal $\delta_{\text{h}}\text{-FAPbI}_3$ as expected. Degradation in this device is seen rapidly as the conversion begins within the first hour of operation under the moderately humid conditions of this experiment. This conversion to the yellow phase is correlated with a reduction in the device performance, particularly the short-circuit current, as this phase has a wide bandgap and thus does not strongly absorb visible light.

The $\text{FA}_{0.85}\text{Cs}_{0.15}\text{PbI}_3$ device composition is tuned to have a tolerance factor within the range to stabilize the photoactive black, cubic $\alpha\text{-FACsPbI}_3$, perovskite phase. Previously, we have shown these samples to have long shelf life stability compared to their pure FA counterpart which we, and others, have attributed to their tolerance factor.¹⁹ The *in-situ* data (figure 1b, and figure 2a) shows that their operational stability is quite different. After approximately 90 minutes, under the stresses of light and humidity, the mixed A-site $\alpha\text{-FA}_{0.85}\text{Cs}_{0.15}\text{PbI}_3$ material partially phase segregates into its constituent phases: “yellow” hexagonal $\delta_{\text{h}}\text{-FAPbI}_3$, and orthorhombic $\delta_{\text{o}}\text{-CsPbI}_3$. This results in loss of device performance, particularly photocurrent, which is slower but similar to that seen in pure FAPbI_3 as these phases are not photo-active.

To further explore the stability of mixed A-site PSCs we performed *in-situ* measurements on a $\text{FA}_{0.758}\text{MA}_{0.152}\text{Cs}_{0.091}\text{PbI}_3$ device (figure 1c,d and figure 2b). The sample composition of this ternary mixed A-site film is such that the lattice spacing, and thus the Goldschmidt tolerance factor, closely mirrors that of the $\text{FA}_{0.85}\text{Cs}_{0.15}\text{PbI}_3$ (Figure S10). Keeping the tolerance factor nearly identical between the two materials by judiciously selecting the compositions allows us to rule out gross differences in stability related to geometric tolerance factor arguments. This more complex ternary cation mixture shows much greater operational stability and resistance to phase segregation. Figure 1d shows the XRD profile of the $\text{FA}_{0.758}\text{MA}_{0.152}\text{Cs}_{0.091}\text{PbI}_3$ device after 15 hours. From this data we can see only very weak peaks associated with the phase segregation into the “yellow” $\delta_{\text{h}}\text{-FAPbI}_3$, and $\delta_{\text{o}}\text{-CsPbI}_3$ phases. Figure 2b shows that this improved phase stability does indeed appear to translate to improved device stability, clearly shown by the slowed photocurrent decay, though of course the design of the surrounding device layers also impact stability under these conditions.⁴⁰ Complementary *ex-situ* device performance and stability characterization of perovskite active layers with the same compositions measured *in-situ* are shown in figure S9 for comparison and display a similar stability trend as that seen during the *in-situ* measurements presented in figures 2. However, we would like to note that the shape of the *in-situ* IV curves appears to be a result of electrical contact issues resulting due to the complex setup required for the *in-situ* experiments (figure S1) which requires the contacts to be placed in a way to not obstruct the x-ray scattering signal. When measured *ex-situ* in a conventional testing setup these same devices perform as expected with low series resistance and high shunt resistance (figure S3, table S1, and figure S9).

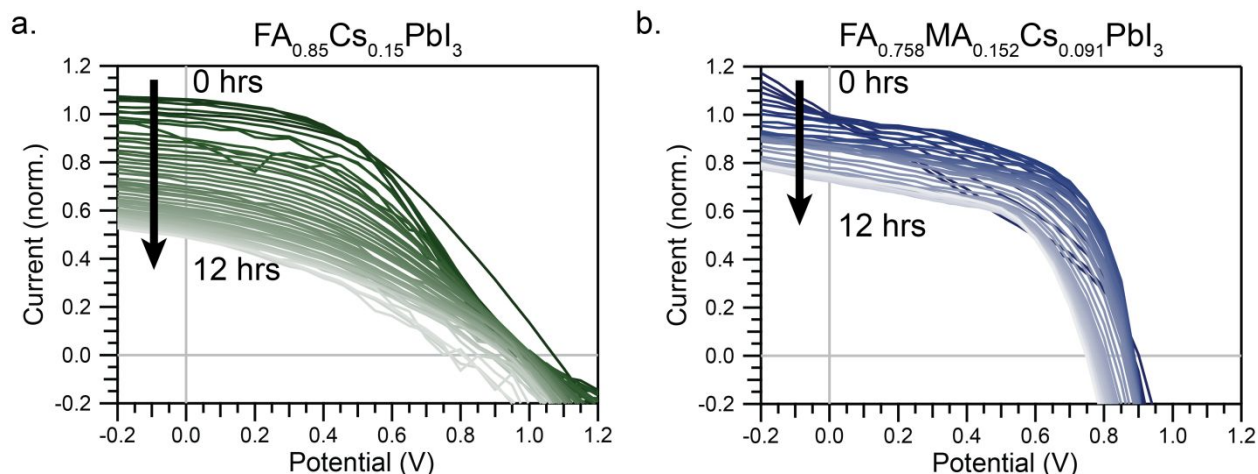


Figure 2: Device performance degradation vs time. Reverse scan IV curves for (a) $FA_{0.85}Cs_{0.15}PbI_3$ and (b) $FA_{0.758}MA_{0.152}Cs_{0.091}PbI_3$ devices taken in-situ. Devices from this sample set had initial recorded PCE of $\sim 18\%$ for the $FA_{0.85}Cs_{0.15}PbI_3$ and $\sim 16\%$ for $FA_{0.758}MA_{0.152}Cs_{0.091}PbI_3$ the reverse direction J-V characterized ex-situ at NREL and shown in the figure S3 and summarized in Table S1.

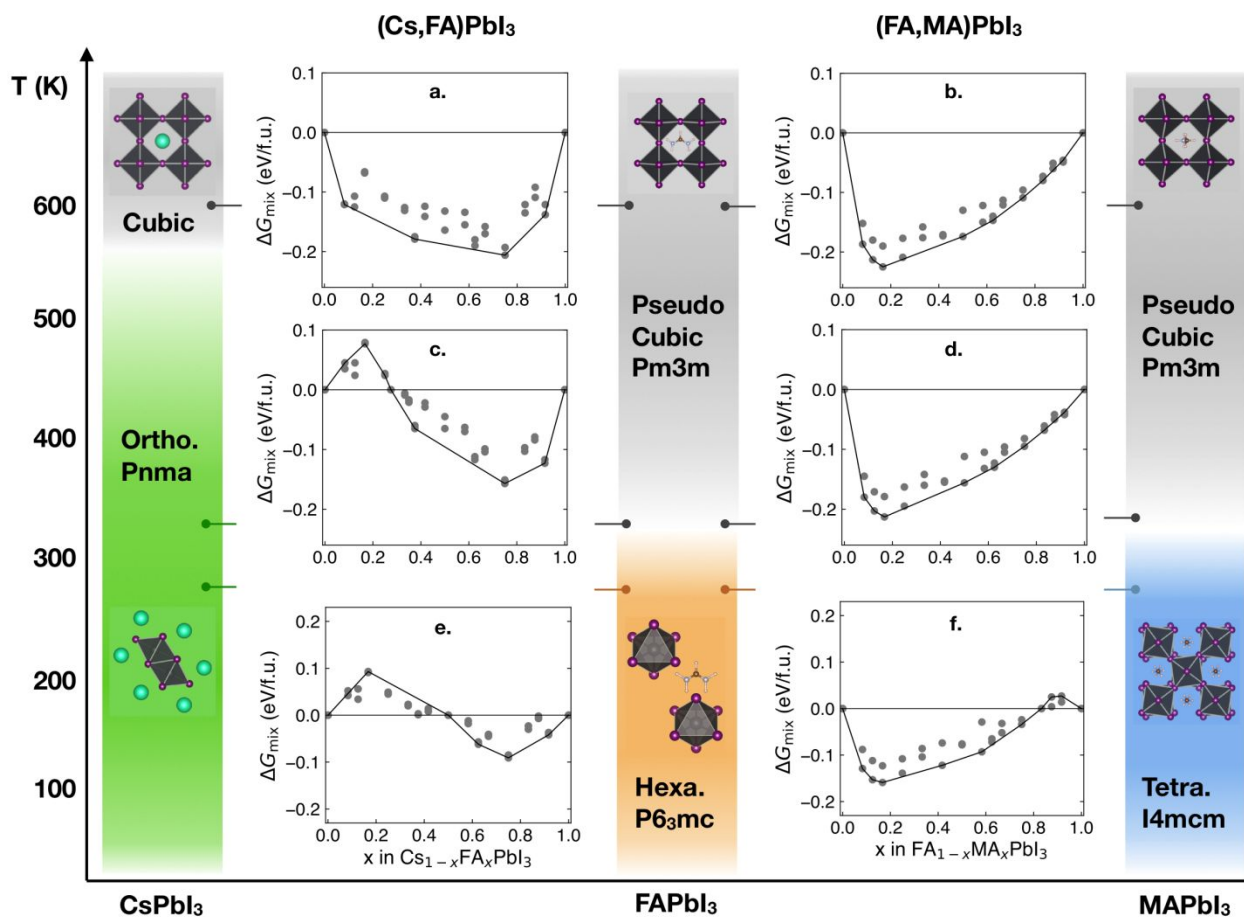


Figure 3. DFT calculated thermodynamics of mixing of mixed A-site halide perovskites. Calculated/Modeled Gibbs free energy of mixing ($\Delta G_{mix} = \Delta E_{mix} - T\Delta S_{mix}$) for $Cs_{1-x}FA_xPbI_3$ and $FA_{1-x}MA_xPbI_3$.

$x\text{MA}_x\text{PbI}_3$ in the assumed pseudo-cubic structure as a function of A-site composition (x) is shown. Details on how we model temperature dependence to Gibbs free energy of mixing is provided in the text and SI. Briefly, for a given A-site composition, Gibbs free energy of mixing (ΔG_{mix}) is calculated with respect to the constituent, or pure, phases in different crystal structures. The phase transition temperature of constituent phases are obtained from refs^{41–43}. For each A-site composition more than one structure, varying in the orientation of the FA and or MA molecules in the lattice, is simulated in DFT calculations (represented by dots on the plot).

To better understand the stability of these mixed A-site halide perovskites we have computed the Gibbs free energy of mixing ($\Delta G_{\text{mix}} = \Delta H_{\text{mix}} - T\Delta S_{\text{mix}}$) of these materials as a function of A-site composition (figure 3). A negative value for ΔG_{mix} , suggests that the constituent phases will readily mix into each other to form a stable mixture. The modeled ΔG_{mix} has two components, (1) Enthalpy of mixing, and (2) Entropy of mixing. Enthalpy of mixing (ΔH_{mix}) is calculated from density functional theory (DFT) by taking the difference between the total energy of the mixed A-site halide perovskite with respect to the total energy of the constituent, or pure, phases (Eq.S3 in SI). The calculations on the mixed A-site halide perovskites assume a pseudocubic crystal structure with random distribution of atoms at the A-site modeled using the special quasi-random structure (SQS) approach.⁴⁴ All SQS structures are fully relaxed (all cell parameters as well as the atomic positions) within DFT calculations and following the relaxations mixed A-site structures at various compositions are found to retain the overall cubic symmetry (Figure S2). The temperature dependence ($T\Delta S_{\text{mix}}$) to Gibbs free energy is incorporated by only considering the entropic contributions associated with the configurational and rotational degrees of freedom (Eq.S5 in SI). The phonons are assumed to not contribute appreciably to the ΔG_{mix} , i.e. it is approximated that the phonons contributions are similar in magnitude between the mixed A-site halide perovskites and the constituent phases and therefore cancel to a large degree when computing thermodynamics of mixing.⁴⁵ We note that the binary $\text{FA}_{1-x}\text{MA}_x\text{PbI}_3$ system is energetically very similar to the $\text{MA}_x\text{FA}_y\text{Cs}_{1-x-y}\text{PbI}_3$ ternary mixture. In order to better visualize the thermodynamics of mixed A-site halide perovskites, we first will present the results of the binary mixtures (Figure 3). Finally, we will discuss these results in context with the calculations of the $\text{MA}_x\text{FA}_y\text{Cs}_{1-x-y}\text{PbI}_3$ ternary mixture.

Calculations show that the free energy of mixing for both $\text{FA}_{1-x}\text{Cs}_x\text{PbI}_3$ and $\text{FA}_{1-x}\text{MA}_x\text{PbI}_3$ in the photo-active cubic, perovskite structure is significantly negative (figure 3a and 3b) at high temperatures ($T \geq 600$ K) for the whole range of A-site compositions. Based on our calculations we find that $\text{FA}_{1-x}\text{Cs}_x\text{PbI}_3$ perovskite phase has large negative enthalpy of mixing with respect to the cubic constituent phases, and its stability is not driven by entropy changes as previously suggested.²² This large negative enthalpy of mixing suggests that the constituent phases will readily mix into each other to form a complete homogenous mixture at high temperature. These calculations then indicate that processing involving annealing, should be done at temperatures at which the pure end point compositions have the same crystal structure in order to have ideal mixing and production of uniform films. The current desire for homogeneity is presumed due to the impact of compositional disorder on the electronic structure of the film. It is of note that, for both binary A-site compositions, the largest free energy gain, in the order of 200 meV/f.u., is found

to occur for FA-rich compositions. Further, as the mixed A-site halide perovskite is cooled to room temperature its stability can change because now the phase equilibrium needs to be established between the mixed A-site halide perovskite in the cubic phase with respect to its constituent phases in their stable low temperature structures.

Next for the purpose of investigating the room temperature stability of the mixed A-site halide perovskites at various compositions, we evaluate ΔG_{mix} slightly above $T=300$ K with respect to the orthorhombic CsPbI_3 and cubic FAPbI_3 and MAPbI_3 , and slightly below $T=300$ K with respect to the hexagonal FAPbI_3 , tetragonal MAPbI_3 and orthorhombic CsPbI_3 . Slightly above 300 K, the thermodynamics of mixing of the $\text{FA}_{1-x}\text{Cs}_x\text{PbI}_3$ mixed A-site halide perovskite relative to the orthorhombic CsPbI_3 and cubic FAPbI_3 changes (figure 3c) such that the mixed A-site phase is now energetically stable ($\Delta G_{\text{mix}} < 0$) only for compositions with the FA mole fraction larger than 0.33. For Cs-rich compositions ($x < 0.33$) the mixed A-site phase has a positive enthalpy of mixing that will drive the system to phase segregate into the orthorhombic CsPbI_3 and FA-rich $\text{FA}_{1-x}\text{Cs}_x\text{PbI}_3$. This suggests that local structural inhomogeneity can drive the mixture to phase segregate placing a premium on establishing a homogeneous film and quenching it before segregation can occur. Previous experiments¹⁹ have found that the mixed A-site FACs at the Cs-rich composition adopts the orthorhombic structure rather than the cubic, at temperatures above 300 K, which is consistent with our predictions. $\text{FA}_{1-x}\text{MA}_x\text{PbI}_3$ in the cubic structure however, remains energetically stable (negative ΔG_{mix}) at $T \geq 300$ K for the whole range of A-site compositions with cubic FAPbI_3 and MAPbI_3 being the constituent phases (figure 3d), which is also consistent with the experimentally observed solubility and the cubic structure of $\text{FA}_{1-x}\text{MA}_x\text{PbI}_3$ studied here (Figure 1c).

To analyze the phase stability below 300 K, we calculate the Gibbs free energy of mixing of mixed A-site halide perovskite in the cubic structure (figure 3e and 3f) with respect to the constituent phases in their ground state structures, that is, relative to orthorhombic CsPbI_3 , hexagonal FAPbI_3 and tetragonal MAPbI_3 . The $\text{FA}_{1-x}\text{MA}_x\text{PbI}_3$ mixture remains stable for the larger part of the compositional range with $\Delta G_{\text{mix}} = -159$ meV/f.u. at the FA-rich ($x=0.17$) side. The $\text{FA}_{1-x}\text{Cs}_x\text{PbI}_3$ on the other hand is relatively less stable than $\text{FA}_{1-x}\text{MA}_x\text{PbI}_3$ below $T=300$ K with the minimum $\Delta G_{\text{mix}} = -91$ meV/f.u. at $x=0.75$. At the composition studied here (Figure 1b, $x=0.85$) the calculated Gibbs free energy of mixing of the $\text{FA}_{1-x}\text{Cs}_x\text{PbI}_3$ is even less negative (about -47 meV/f.u.). The fact that FA rich composition ($x=0.85$) is stable to synthesize experimentally is consistent with the predicted negative Gibbs free energy of mixing, and it is likely that over time exposure to sunlight and/or phonon contributions could be sufficient to drive the cubic mixed A-site $\text{FA}_{0.85}\text{Cs}_{0.15}\text{PbI}_3$ to phase segregate into its constituent phases, hexagonal FAPbI_3 and orthorhombic CsPbI_3 , and deteriorate the device performance when compared to the much more stable homogeneous phase of the $\text{FA}_{1-x}\text{MA}_x\text{PbI}_3$.

In addition to the binary mixed A-site halide perovskites, we also modeled ΔG_{mix} for the $\text{MA}_x\text{FA}_y\text{Cs}_{1-x-y}\text{PbI}_3$ ternary mixture in the cubic structure at specific compositions of interest (see figure S11). The Gibbs free energy of mixing in $\text{FA}_{0.75}\text{MA}_{0.167}\text{Cs}_{0.083}\text{PbI}_3$ ($\Delta G_{\text{mix}} \approx -180$ meV/unit) is similar to the $\text{FA}_{1-x}\text{MA}_x\text{PbI}_3$ binary mixture, $\text{FA}_{0.833}\text{MA}_{0.167}\text{PbI}_3$ when compared to the cubic FAPbI_3 and MAPbI_3 at temperature slightly above 300 K. Similar to the previous comparison of

the binary A-site mixtures, the ternary $\text{FA}_{0.75}\text{MA}_{0.167}\text{Cs}_{0.083}$ ($\Delta G_{\text{mix}} = -102$ meV/unit) is also found to be much more stable than the mixed A-site $\text{FA}_{1-x}\text{Cs}_x\text{PbI}_3$ when compared with the non-cubic constituent phases at temperatures below 300 K. The overall gain in the Gibbs free energy of mixing for the $\text{MA}_x\text{FA}_y\text{Cs}_{1-x-y}\text{PbI}_3$ ternary is larger than the $\text{FA}_{1-x}\text{Cs}_x\text{PbI}_3$ binary. Therefore, we hypothesize that this gain in free energy will help stabilize the cubic ternary much more than the $\text{FA}_{1-x}\text{Cs}_x\text{PbI}_3$ binary to temperatures lower than the transition temperatures (around 300 K) of the constituent phases. These predictions are also consistent with the experimental work presented here (see Figure 1 and Figure S4) showing improved structural stability of the ternary $\text{MA}_x\text{FA}_y\text{Cs}_{1-x-y}\text{PbI}_3$ compared to binary $\text{FA}_{1-x}\text{Cs}_x\text{PbI}_3$ mixed A-site halide perovskites. This theory prediction is also consistent with other experiments confirming better stability of a $\text{MA}_x\text{FA}_y\text{Cs}_{1-x-y}\text{PbI}_3$ ternary mixture over a $\text{FA}_{1-x}\text{MA}_x\text{PbI}_3$ binary mixture²¹, and better stability of the binary $\text{FA}_{1-x}\text{MA}_x\text{PbI}_3$ over pure FAPbI_3 .⁴⁶

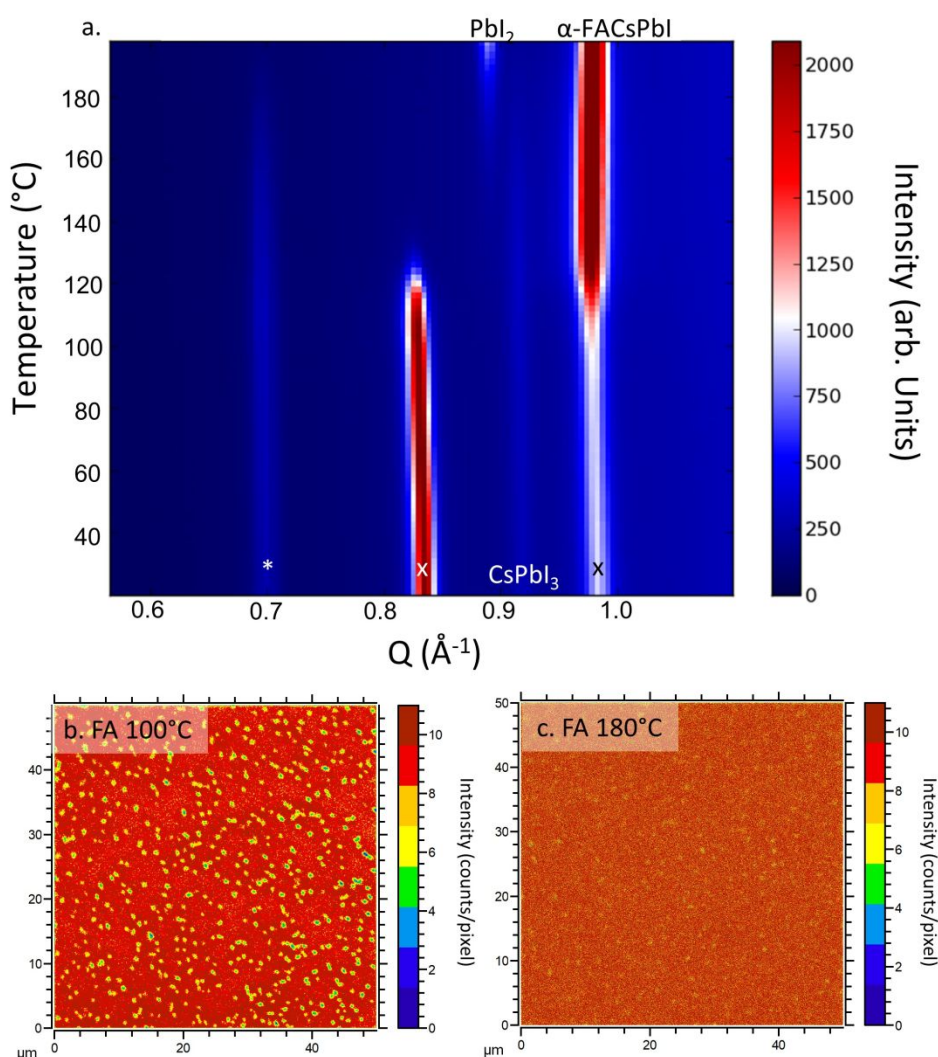


Figure 4: In situ annealing of $\text{FA}_{0.7}\text{Cs}_{0.3}\text{PbI}_3$ and TOF-SIMS. (a) The observed phases are labeled on the plot, the peaks at 0.82, and 0.98 \AA^{-1} are associated with the precursor phase

(marked by x) and the peak at 0.7 \AA^{-1} is associated with a hydrate phase (marked by *). TOF-SIMS mapping of FA in films exposed to (a) $100 \text{ }^\circ\text{C}$ and (b) $180 \text{ }^\circ\text{C}$.

The XRD experiments reported above, during aging, show how the mixed A-site PSCs can demix, consistent with our theoretical calculations. To further validate these theoretical calculations we choose to explore the route these materials take during formation to better understand the initial mixing of FA and Cs in the as formed films. *In situ* XRD during annealing of a $\text{FA}_{0.70}\text{Cs}_{0.30}\text{PbI}_3$ film is shown in figure 4a. Initially the XRD data show the presence of a precursor phase, which is likely a complex structure containing dimethyl sulfoxide (DMSO) solvent molecules (0.82 , and 0.98 \AA^{-1}), and $\delta_0\text{-CsPbI}_3$ 0.92 \AA^{-1} . The $\delta_0\text{-CsPbI}_3$ phase persists past the disappearance of the precursor peak at 0.82 \AA^{-1} at $122 \text{ }^\circ\text{C}$. This CsPbI_3 eventually mixes with the FAPbI_3 phase at $160 \text{ }^\circ\text{C}$ consistent with our theory calculations. To explore the spatial composition of these mixed A-site PSCs we use time of flight secondary ion mass spectrometry (TOF-SIMS) which has been shown to be a useful tool in determining the spatial distribution of the PSC subunits.⁴⁷ TOF-SIMS tomography data (figure 4b, figure S12) shown for a $\text{FA}_{0.70}\text{Cs}_{0.30}\text{PbI}_3$ film annealed using the same conditions as the *in situ* XRD (figure 4a), show clear differences in the homogeneity of the cations as a function of processing temperature ($100 \text{ }^\circ\text{C}$ and $180 \text{ }^\circ\text{C}$). The data show a clear decrease in heterogeneity as the process temperature is elevated which is evident visually. Analysis of the distribution for FA and Cs is consistent with improved homogeneity and the improved mixing apparent visually. To further validate the theoretical calculations we performed TOF-SIMS on an annealed $\text{FA}_{0.75}\text{MA}_{0.167}\text{Cs}_{0.083}\text{PbI}_3$ film (figure S12). As predicted by theory we observe a homogenous distribution of the A-site atoms. These data also validate the ability of theory calculations to aid in the choice of process conditions to realize more homogeneous uniform films, consistent with the observed phases in the XRD.

Conclusions:

In light of the theory-driven predictions derived in this work, we can explain the new experimental data presented here, as well as that in older reports regarding mixed A-site PSCs.¹⁹ The guiding principal which results, is that the ability to create a homogeneously mixed film depends on both the end member structures as well as the stable phase of the mixed A-site PSC at the processing temperature during film formation. This principle, exposed by theory, is consistent not only with the experimental data presented here but also with other experimental observations using XRD and TOF-SIMS in which structural/compositional inhomogeneity is observed in as deposited and subsequent operated devices.^{47,48} We note that other considerations such as the solvent, stoichiometric variation, and the atmospheric chemistry, which can modulate the mobility of the different components within the film, along with the extent to which mixing or segregation is allowed prior to rapid quenching of the film into a fixed metastable state, are also crucial. We also note other studies by photoluminescence (PL) and IR imaging that indicate in homogeneity at smaller lengthscales which are reported to appear in as deposited films which again point to the processing details playing an important role.⁴³ Similarly we anticipate that similar although perhaps somewhat modified considerations will govern systems in which mixed halides are used (e.g. $\text{FA}_{1-\alpha-\beta}\text{MA}_\alpha\text{Cs}_\beta\text{PbI}_{3-x}\text{Br}_x$ compounds). Taken together, these observations emphasize the importance of processing and compositional choices when developing stable active layer materials.

In summary, we have presented a deeper look into the behavior of mixed A-site PSCs under operational conditions. We observe a greater structural instability (phase segregation) in the binary $\text{FA}_{0.85}\text{Cs}_{0.15}\text{PbI}_3$ compared to the ternary, $\text{FA}_{0.758}\text{MA}_{0.152}\text{Cs}_{0.091}\text{PbI}_3$, with near-identical tolerance factor. With DFT we calculate the Gibb's free energy of mixing for these mixed A-site halide perovskites and show the role of local structure in the mixing/stability of these PSCs by validating predictions of de-mixing from these calculations using in situ XRD and TOF-SIMS measurements. This work highlights the importance of the thermodynamic behavior of these complex mixed A-site PSCs, and the insight which understanding the thermodynamic landscape can provide when designing new device materials and fabrication processes. By using this experimentally validated theoretical perspective it is thus possible to target real and relevant processing strategies that will produce well-mixed structures, which are expected to have improved stability and performance.

Acknowledgements: The authors wish to thank Fei Zhang for providing samples for TOF-SIMS analysis. This work was supported by the U.S. Department of Energy (DOE) Solar Energy Technology Office (SETO) of the Energy Efficiency and Renewable Energy (EERE) award for the Hybrid and Perovskite Solar Cell (HPSC) project at the National Renewable Energy Laboratory under Contract No DE-AC36-08-GO28308 managed and operated by the Alliance for Sustainable Energy, LLC. Theory portions of this research used computational resources sponsored by the DOE Office of Energy Efficiency and Renewable Energy and located at the National Renewable Energy Laboratory. Use of the Stanford Synchrotron Radiation Lightsource, SLAC National Accelerator Laboratory, was supported by the U.S. Department of Energy, Office of Basic Energy Sciences under Contract No. DE-AC02-76SF00515. J.A.C. was supported by the Department of Energy, Office of Energy Efficiency and Renewable Energy Postdoctoral Research Award under contract number DE-SC00014664. The views expressed in the article do not necessarily represent the views of the DOE or the U.S. Government. The U.S. Government retains and the publisher, by accepting the article for publication, acknowledges that the U.S. Government retains a nonexclusive, paid-up, irrevocable, worldwide license to publish or reproduce the published form of this work, or allow others to do so, for U.S. Government purposes.

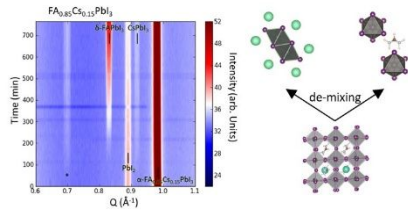
References:

- 1 W. S. Yang, B.-W. Park, E. H. Jung and N. J. Jeon, *Science* (80-.), 2017, **356**, 1376–1379.
- 2 National Renewable Energy Laboratory, NREL Chart, http://www.nrel.gov/ncpv/images/efficiency_chart.jpg.
- 3 Z. Li, T. R. Klein, D. H. Kim, M. Yang, J. J. Berry, M. F. A. M. Van Hest and K. Zhu, *Nat. Rev. Mater.*, 2018, **3**, 1–20.
- 4 G. E. Eperon, S. D. Stranks, C. Menelaou, M. B. Johnston, L. M. Herz and H. J. Snaith, *Energy Environ. Sci.*, 2014, **7**, 982.
- 5 M. L. Petrus, J. Schlipf, C. Li, T. P. Gujar, N. Giesbrecht, P. Müller-Buschbaum, M. Thelakkat, T. Bein, S. Hüttner and P. Docampo, *Adv. Energy Mater.*, 2017, **7**, 1700264.
- 6 L. K. Ono, M. R. Leyden, S. Wang and Y. Qi, *J. Mater. Chem. A*, 2016, **4**, 6693–6713.
- 7 A. Sharenko and M. F. Toney, *J. Am. Chem. Soc.*, 2016, **138**, 463–470.

- 8 Z. Xiao, Y. Yuan, Q. Wang, Y. Shao, Y. Bai, Y. Deng, Q. Dong, M. Hu, C. Bi and J. Huang, *Mater. Sci. Eng. R Reports*, 2016, **101**, 1–38.
- 9 Q. Chen, N. De Marco, Y. (Michael) Yang, T.-B. Song, C.-C. Chen, H. Zhao, Z. Hong, H. Zhou and Y. Yang, *Nano Today*, 2015, **10**, 355–396.
- 10 N.-G. Park, *CrystEngComm*, 2016, **18**, 5977–5985.
- 11 Y. Zhou and N. P. Padture, *ACS Energy Lett.*, 2017, **2**, 2166–2176.
- 12 N.-G. Park, *Inorg. Chem.*, 2017, **56**, 3–10.
- 13 J. A. Christians, P. Schulz, J. S. Tinkham, T. H. Schloemer, S. P. Harvey, B. J. Tremolet De Villers, A. Sellinger, J. J. Berry and J. M. Luther, *Nat. Energy*, 2018, **3**, 68–74.
- 14 A. Rajagopal, K. Yao and A. K. Y. Jen, *Adv. Mater.*, 2018, **30**, 1–45.
- 15 K. Domanski, E. A. Alharbi, A. Hagfeldt, M. Grätzel and W. Tress, *Nat. Energy*, 2018, **3**, 61–67.
- 16 A. R. Bowring, L. Bertoluzzi, B. C. O'Regan and M. D. McGehee, *Adv. Energy Mater.*, 2018, **8**, 1–7.
- 17 C. Eames, J. M. Frost, P. R. F. Barnes, B. C. O'Regan, A. Walsh and M. S. Islam, *Nat. Commun.*, 2015, **6**, 7497.
- 18 J. A. Christians, S. N. Habisreutinger, J. J. Berry and J. M. Luther, *ACS Energy Lett.*, 2018, 2136–2143.
- 19 Z. Li, M. Yang, J. S. Park, S. H. Wei, J. J. Berry and K. Zhu, *Chem. Mater.*, 2016, **28**, 284–292.
- 20 M. Saliba, T. Matsui, K. Domanski, J.-Y. Seo, A. Ummadisingu, S. M. Zakeeruddin, J.-P. Correa-Baena, W. R. Tress, A. Abate, A. Hagfeldt and M. Grätzel, *Science (80-.)*, 2016, **354**, 206–209.
- 21 M. Saliba, T. Matsui, J.-Y. Seo, K. Domanski, J.-P. Correa-Baena, M. K. Nazeeruddin, S. M. Zakeeruddin, W. Tress, A. Abate, A. Hagfeldt and M. Grätzel, *Energy Environ. Sci.*, 2016, **9**, 1989–1997.
- 22 C. Yi, J. Luo, S. Meloni, A. Boziki, N. Ashari-Astani, C. Grätzel, S. M. Zakeeruddin, U. Röthlisberger and M. Grätzel, *Energy Environ. Sci.*, 2015, **9**, 656–662.
- 23 J. W. Lee, D. H. Kim, H. S. Kim, S. W. Seo, S. M. Cho and N. G. Park, *Adv. Energy Mater.*, DOI:10.1002/aenm.201501310.
- 24 G. Kieslich, S. Sun and A. K. Cheetham, *Chem. Sci.*, 2014, **5**, 4712–4715.
- 25 S. Draguta, J. A. Christians, Y. V. Morozov, A. Mucunzi, J. S. Manser, P. V. Kamat, J. M. Luther and M. Kuno, *Energy Environ. Sci.*, 2018, **11**, 960–969.
- 26 J. H. Noh, S. H. Im, J. H. Heo, T. N. Mandal and S. Il Seok, *Nano Lett.*, 2013, **13**, 1764–1769.
- 27 A. Sadhanala, F. Deschler, T. H. Thomas, S. E. Dutton, K. C. Goedel, F. C. Hanusch, M. L. Lai, U. Steiner, T. Bein, P. Docampo, D. Cahen and R. H. Friend, *J. Phys. Chem. Lett.*, 2014, **5**, 2501–2505.
- 28 K. A. Bush, A. F. Palmstrom, Z. J. Yu, M. Boccard, R. Cheacharoen, J. P. Mailoa, D. P. McMeekin, R. L. Z. Hoyer, C. D. Bailie, T. Leijtens, I. M. Peters, M. C. Minichetti, N. Rolston, R. Prasanna, S. Sofia, D. Harwood, W. Ma, F. Moghadam, H. J. Snaith, T. Buonassisi, Z. C. Holman, S. F. Bent and M. D. McGehee, *Nat. Energy*, 2017, **2**, 1–7.
- 29 T. Duong, Y. L. Wu, H. Shen, J. Peng, X. Fu, D. Jacobs, E. C. Wang, T. C. Kho, K. C. Fong, M. Stocks, E. Franklin, A. Blakers, N. Zin, K. McIntosh, W. Li, Y. B. Cheng, T. P. White, K. Weber and K. Catchpole, *Adv. Energy Mater.*, 2017, **7**, 1–11.
- 30 A. Goyal, S. McKechnie, D. Pashov, W. Tumas, M. Van Schilfgaarde and V. Stevanović, *Chem. Mater.*, 2018, **30**, 3920–3928.
- 31 A. J. Barker, A. Sadhanala, F. Deschler, M. Gandini, S. P. Senanayak, P. M. Pearce, E. Mosconi, A. J. Pearson, Y. Wu, A. R. Srimath Kandada, T. Leijtens, F. De Angelis, S. E. Dutton, A. Petrozza and R. H. Friend, *ACS Energy Lett.*, 2017, **2**, 1416–1424.
- 32 E. T. Hoke, D. J. Slotcavage, E. R. Dohner, A. R. Bowring, H. I. Karunadasa and M. D.

- McGehee, *Chem. Sci.*, 2015, **6**, 613–617.
- 33 D. J. Slotcavage, H. I. Karunadasa and M. D. McGehee, *ACS Energy Lett.*, 2016, **1**, 1199–1205.
- 34 M. C. Brennan, S. Draguta, P. V. Kamat and M. Kuno, *ACS Energy Lett.*, 2018, **3**, 204–213.
- 35 F. Xu, T. Zhang, G. Li and Y. Zhao, *J. Mater. Chem. A*, 2017, **5**, 11450–11461.
- 36 J. P. Correa Baena, L. Steier, W. Tress, M. Saliba, S. Neutzner, T. Matsui, F. Giordano, T. J. Jacobsson, A. R. Srimath Kandada, S. M. Zakeeruddin, A. Petrozza, A. Abate, M. K. Nazeeruddin, M. Grätzel and A. Hagfeldt, *Energy Environ. Sci.*, 2015, **8**, 2928–2934.
- 37 K. Domanski, B. Roose, T. Matsui, M. Saliba, S. H. Turren-Cruz, J. P. Correa-Baena, C. R. Carmona, G. Richardson, J. M. Foster, F. De Angelis, J. M. Ball, A. Petrozza, N. Mine, M. K. Nazeeruddin, W. Tress, M. Grätzel, U. Steiner, A. Hagfeldt and A. Abate, *Energy Environ. Sci.*, 2017, **10**, 604–613.
- 38 L. T. Schelhas, J. A. Christians, J. J. Berry, M. F. Toney, C. J. Tassone, J. M. Luther and K. H. Stone, *ACS Energy Lett.*, 2016, **1**, 1007–1012.
- 39 R. L. Z. Hoyer, P. Schulz, L. T. Schelhas, A. M. Holder, K. H. Stone, J. D. Perkins, D. Vigil-Fowler, S. Siol, D. O. Scanlon, A. Zakutayev, A. Walsh, I. C. Smith, B. C. Melot, R. C. Kurchin, Y. Wang, J. Shi, F. C. Marques, J. J. Berry, W. Tumas, S. Lany, V. Stevanović, M. F. Toney and T. Buonassisi, *Chem. Mater.*, 2017, **29**, 1964–1988.
- 40 M. O. Reese, S. A. Gevorgyan, M. Jørgensen, E. Bundgaard, S. R. Kurtz, D. S. Ginley, D. C. Olson, M. T. Lloyd, P. Morvillo, E. A. Katz, A. Elschner, O. Haillant, T. R. Currier, V. Shrotriya, M. Hermenau, M. Riede, K. R. Kirov, G. Trimmel, T. Rath, O. Inganäs, F. Zhang, M. Andersson, K. Tvingstedt, M. Lira-Cantu, D. Laird, C. McGuinness, S. Gowrisanker, M. Pannone, M. Xiao, J. Hauch, R. Steim, D. M. DeLongchamp, R. Rösch, H. Hoppe, N. Espinosa, A. Urbina, G. Yaman-Uzunoglu, J. B. Bonekamp, A. J. J. M. Van Breemen, C. Girotto, E. Voroshazi and F. C. Krebs, *Sol. Energy Mater. Sol. Cells*, 2011, **95**, 1253–1267.
- 41 C. C. Stoumpos, C. D. Malliakas and M. G. Kanatzidis, *Inorg. Chem.*, 2013, **52**, 9019–9038.
- 42 T. Chen, B. J. Foley, C. Park, C. M. Brown, L. W. Harriger, J. Lee, J. Ruff, M. Yoon, J. J. Choi and S. H. Lee, *Sci. Adv.*, 2016, **2**, 1–7.
- 43 D. H. Fabini, T. A. Siaw, C. C. Stoumpos, G. Laurita, D. Olds, K. Page, J. G. Hu, M. G. Kanatzidis, S. Han and R. Seshadri, *J. Am. Chem. Soc.*, 2017, **139**, 16875–16884.
- 44 A. Zunger, S.-H. Wei, L. G. Ferreira and J. E. Bernard, *Phys. Rev. Lett.*, 1990, **96**, 312–318.
- 45 A. van de Walle and G. Ceder, *Rev. Mod. Phys.*, 2002, **74**, 11–45.
- 46 B. Charles, J. Dillon, O. J. Weber, M. S. Islam and M. T. Weller, *J. Mater. Chem. A*, 2017, **5**, 22495–22499.
- 47 S. Harvey, Z. Li, J. A. Christians, K. Zhu, J. M. Luther and J. J. Berry, *ACS Appl. Mater. Interfaces*, , DOI:10.1021/acsmi.8b07937.
- 48 R. Chatterjee, I. M. Pavlovetc, K. Aleshire, G. V. Hartland and M. Kuno, *ACS Energy Lett.*, 2018, **3**, 469–475.

TOC Graphic:



TOC Text:

The structural stability of mixed A-site perovskite solar cells during operation is observed by *in-situ* XRD and the de-mixing behavior is described by calculating the Gibbs free energy of mixing.